

SUPPORTING INFORMATION

Highly-effective gating of single-molecule junctions: an electrochemical approach.

Masoud Baghernejad,^{a,#} David Zsolt Manrique,^{b,#} Chen Li,^a Thomas Pope,^b Ulmas Zhumaev,^a Ilya Pobelov,^a Pavel Moreno-García,^a Veerabhadrrao Kaliginedi,^a Cancan Huang,^a Wenjing Hong^{a,*}, Colin J Lambert^{b,*}, and Thomas Wandlowski^a

^a Department of Chemistry and Biochemistry, University of Bern, Freiestrasse 3, CH-3012, Bern, Switzerland

^b Department of Physics, Lancaster University, Lancaster LA1 4YB, United Kingdom

Contents:

1. Experimental

1.1 Conductance measurements of single-molecule junction

1.2 Data analysis

2. Results

2.1 Single-molecule junction conductance

2.2 Junction formation and evolution

2.3 Electrochemical gate effect at different pH values

2.4 π - π Stacking evolution

2.5 Comparison of gating efficiency with literature data

3. DFT based electron transport calculations

4. References

1. Experimental

1.1 Conductance measurements of single-molecule junction

The conductance measurements of 4,4'-bipyridine (44BPy) single-molecule junction were carried out using electrochemical Scanning Tunneling Microscopy-break Junction (STM-BJ) approach. The current was recorded at fixed bias potential during repeated formation and breaking of molecular junction. The experimental details and instrumentation descriptions were given in our previous publications[1, 2].

The STM sample substrates were a Au(111) single bead crystal. The substrates were freshly flame-annealed prior to use. The gold STM tips were prepared by electrochemical etching of gold wires (99.999%, 0.5 mm diameter) in a 1:1 (v/v) mixture of 30% HCl and ethanol. All the organic chemicals were purchased from Sigma-Aldrich and used without further purification. The solutions containing 5mM or 0.1 mM 44BPy were used for all the experiments. All the experiments were carried out in room temperature in an argon atmosphere.

In the electrochemical controlled experiments, the gold STM tips were coated with polyethylene to ensure that the leakage current was smaller than 1~2 pA. Pt wires were used as the counter or quasi-reference electrodes [Note: The sample potential values were calibrated later vs. MSE in all the pHs]. The electrolyte solutions were prepared using Milli-Q water (18 M Ω , 2 ppb TOC) with either HClO₄ or KClO₄, and were deoxygenated prior to use. The solution pH was adjusted by adding NaOH solution. All the chemicals were of supra pure grade (Merck). Internal bipotentiostat was used to control the potential of both tip and substrate. The STM images and cyclic voltammograms were recorded frequently during the measurements. The former was used to monitor the cleanness and flatness of Au(111) surface as well as sharpness of the gold tip. The

latter was used to ensure that there is no oxygen in the system and no drift in the reference electrode.

The STM-BJ experiments were performed by a modified Molecular Imaging PicoSPM. The commercial STM scanner was modified with a dual channel preamplifier[2]. The current signal was converted to two voltage signals with the conversion factors $\sim 21 \mu\text{A}/\text{V}$ and $10 \text{ nA}/\text{V}$. Both signals were split to the original as well as the 10 times amplified signal. The custom-designed program drives the STM tip at a controlled rate ($87\text{nm}/\text{s}$) toward the STM substrate when the feedback is switched off. The approaching was stopped for few ms when the upper current limit was reached (e.g. $10 G_0$). The tip is then withdrawn at a controlled rate from the substrate to ensure the completely breaking the molecular junction. This cycle was repeated thousands times for each set of experimental condition. The current-time traces of each cycle (retraction part) were recorded with the digital oscilloscope (Yokogawa DL750).

1.2 Data analysis

The raw data were analyzed with a lab-made program WA-BJ implemented in LabView2011. All the linear channels were combined to an integrated trace after manipulation by a respective gain factor. Finally, all the histograms were generated without any data selection.

2. Results

2.1 Single-molecule junction conductance

The STM-BJ experiments were performed in mesitylene as a non-polar solvent and polar media with different pH values employing HClO_4 and KClO_4 as electrolyte. The current was recorded between the STM gold tip and Au(111) substrate at constant bias voltage 100 mV . The typical

individual conductance traces are shown in Figure S1A. Due to the adhesion of gold atoms, after breaking the gold-gold contact, two electrodes tend to form a gap with a certain distance [3-5] and a sharp decrease in conductance up to 6 orders of magnitude immediately after breaking the gold-gold contact can be seen in these traces. From figures S1A and S1C, it is clear that 44BPy junction forms immediately after breaking the gold-gold contact which tip-sample distance is $6.5 \pm 2.5 \text{ \AA}$ and nitrogen to nitrogen distance is 7.2 \AA [3, 6]. The molecule will bridge onto the gap causing plateaus after sharp decrease in conductance related to breaking gold-gold contact. Additional features, such as plateaus are observed at $G \leq 10^{-3}G_0$, which are attributed to the formation of molecular junctions marked with H' and L'. The noise level is reached at $G < 10^{-6}G_0$ in the STM-BJ experiments. Several thousands of individual G versus Δz traces were recorded and subsequently analysed further by constructing all-data point histograms (without any data selection) to extract statistically significant results. Figure S1B displays the corresponding one-dimensional (1D) histogram of 44BPy in a semi-logarithmic scale. We observed peaks for the breaking of Au-Au contacts, and two well-defined molecular-junction related features. A Gaussian fit led to $G^* = (3.1 \pm 0.2)10^{-5} G_0$ and $(3.8 \pm 0.2)10^{-5} G_0$ as the most probably single molecular junction conductance values of 44BPy. These values appear to be independent on the concentration of 44BPy down to 0.1 mM. The analysis for 1D histogram construction was extended by constructing all-data point two-dimensional (2D) conductance vs. displacement histograms [7, 8]. This representation provides direct access to the evolution of molecular junctions during the formation, stretching and break-down steps.

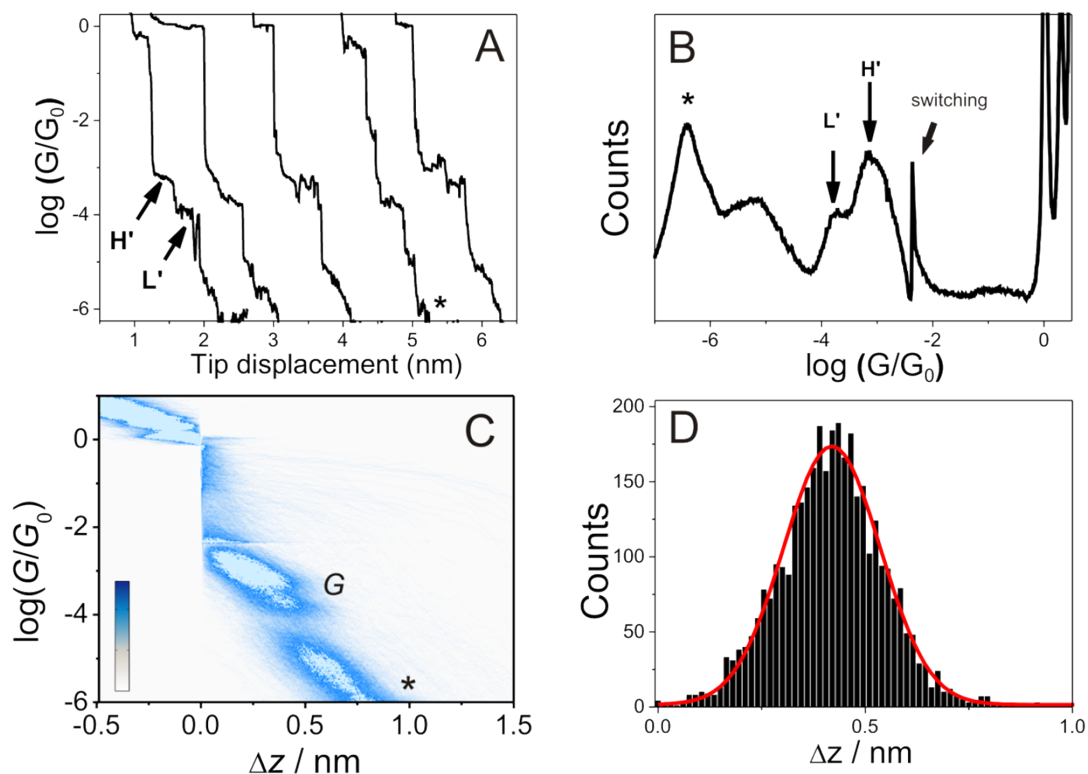


Figure S1. STM-BJ-based conductance measurements of 44BPY in TMB as recorded with $V_{\text{bias}} = 0.100$ V and a stretching rate of 87nm s^{-1} . (A) Typical original conductance vs. distance traces. (B) 1D conductance histogram and (C) 2D conductance histogram generated from 2000 individual curves without any data selection. The noise level is indicated by the asterisk. The small spike at $\log(G/G_0) \approx -2.2$ in panel B represents an artefact related to the switching of the amplifier. (D) Characteristic displacement length histogram[9]

The individual $G - \Delta z$ traces were aligned by setting the common origin to $\Delta z = 0$ and $G = 0.7 G_0$. The data reveal quantized conductance features at $G \geq 1 G_0$. They correspond to the breaking of gold-gold contacts. An additional high-density data cloud is observed in $10^{-2.5}G_0 \leq G \leq 1.0 \cdot 10^{-4.0}G_0$, centered on $10^{-3.1}$ and $10^{-3.8} G_0$. These regions represent the conductance range of a single 44BPY molecule bridging the gold nanoelectrodes. There is also a conductance feature at $10^{-5.0} G_0$, which can be assigned to the stacking molecular junction. The 2D histogram in Figure S1C demonstrates further that the conductance decreases monotonously with increasing relative displacement (or junction elongation) Δz . The high conductance (H') is 3~4 times larger than low conductance (L').

Figure S1D displays the characteristic displacement histograms of 44BPY. The plot shows a uniform normal distribution with a well-defined maximum $\Delta z^* = (0.4 \text{ nm})$ as a measure of the most-probable plateau lengths of 44BPY molecular junctions attributed to all the plateaus. This figure led to the estimate of a junction formation probability of $\sim 100 \%$.

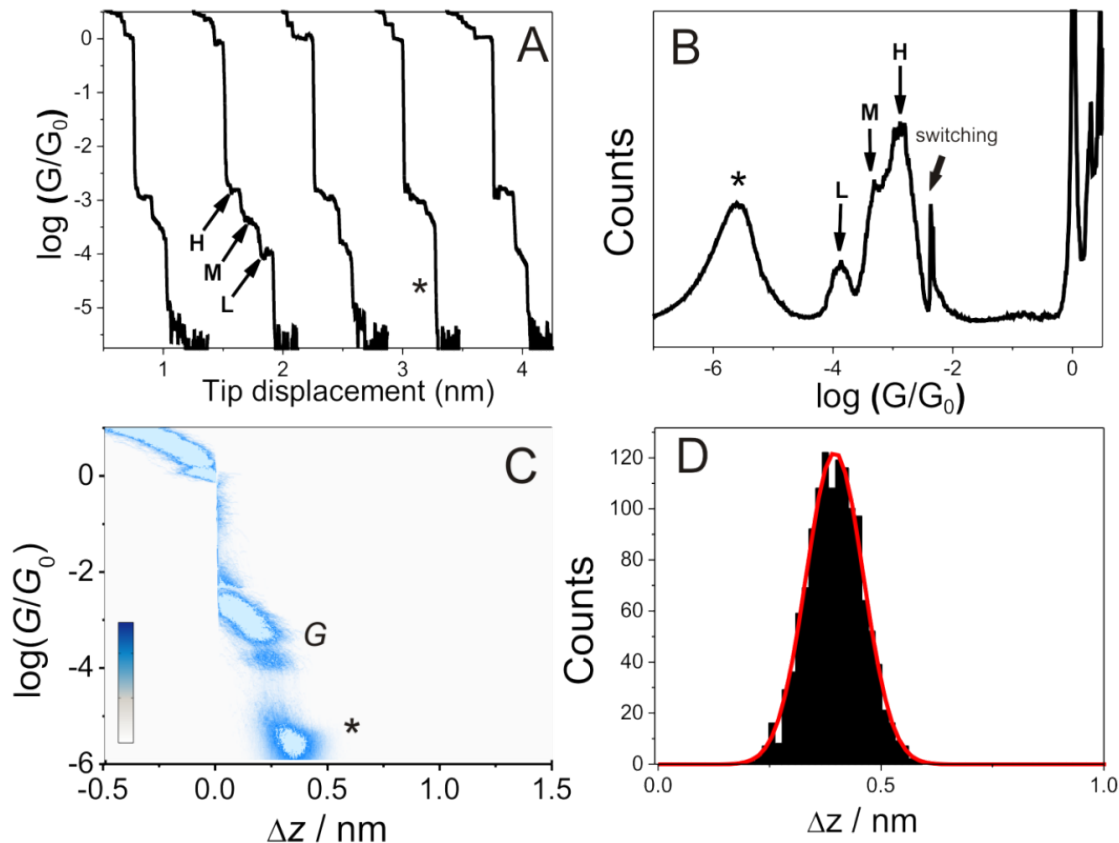


Figure S2. STM-BJ-based conductance measurements of 44BPY in 0.05 M KClO_4 as recorded with $V_{\text{bias}} = 0.100 \text{ V}$ and a stretching rate of 87 nm s^{-1} . (A) Typical original conductance vs. distance traces. (B) 1D conductance histogram and (C) 2D conductance histogram generated from 2000 individual curves without any data selection. The noise level is indicated by the asterisk. The small spike at $\log(G/G_0) \approx -2.2$ in panel B represents an artefact related to the switching of the amplifier. (D) Characteristic displacement length histogram [9].

Next, as it is displayed in figure S2, we investigated the conductance of 44BPY in 0.05 M KClO_4 under potential control. The same strategy as mentioned above was performed for sample conductance traces, 1D, 2D, and plateau length histogram construction. Here three conductance

states can be observed assigned with high (H), Middle (M), and low (L) values with high-density data cloud is observed in $10^{-4.5}G_0 \leq G \leq 1.0 \cdot 10^{-2.5}G_0$, centered on $10^{-2.9}$, $10^{-3.3}$, and $10^{-3.9} G_0$ which is in good agreement with previously reported works [6, 10, 11].

The conductance values measured with various electrochemical potential and it is found that no redox process was observed for 44BPy within the electrochemical potential window we selected for this work. We also note that achieving on-resonance gating with this method is limited as wider potential range would result in high electrochemical current because of hydrogen evolution on the surface of the gold electrodes and it makes the single-molecule conductance measurement impossible.

2.2 Junction formation and evolution

In order to further understand the configuration-conductance relationship, the plateau length for molecule junction was defined within the interval $[10^{-0.5}G_{\text{peak}}, 10^{0.5}G_{\text{peak}}]$, where G_{peak} is the most probable conductance extracted from conductance histogram. Figure S3, shows a series of the plateau length histograms built from the same set of data as the conductance histogram shows in Figure S2D. Obviously, two distinctly different distribution of plateau length are observed. Plateau lengths for H are similar to those of M while this measurement shows different plateau lengths for L but similar to monatomic (G_0). Two different plateau length distributions clarify two different mechanical processes. These plateaus can be created by many different phenomenon like stretching of gold electrodes and molecules, gold atomic rearrangement, sliding of the molecules on the surfaces of the electrodes, and changes in molecular geometry on the contact. Molecule stretching on the surface can be simulated as stretching of a “spring” [5, 12-14] thus the plateau length of G_0 can determine by the spring constant of gold electrode and strength of Au-Au bond (1.5 nN).

Basically, the weaker Au-N bond (0.8 nN) [15, 16] is not sufficient to pull the gold atoms out, therefore no atomic rearrangement is possible at the gold surface and a shorter plateau length is observed comparing to Au-S bond [17]. Accordingly, one may expect H and M conductance values are mainly caused by the sliding of two and one molecules with a tilted geometry on the banks of the electrodes, respectively.

The following interpretation is consistent with our results. A monatomic contact first forms and stretches, causing the G_0 plateau. Since the gaps between electrodes which forms immediately after electrode relaxation is shorter than molecular length, one or two molecules can attach and start to slide to the banks of the electrodes with tilted geometry, causing H and M conductance values. In the case of observing H conductance value, as long as two leads are withdrawing, Au-N bond ruptures and M conductance value can be observed sequentially in most of the sample traces. The further elongation enables the molecule to bond to the apex of the electrodes vertically, causing L plateau. In an ideal case, these events are expected to take place sequentially.

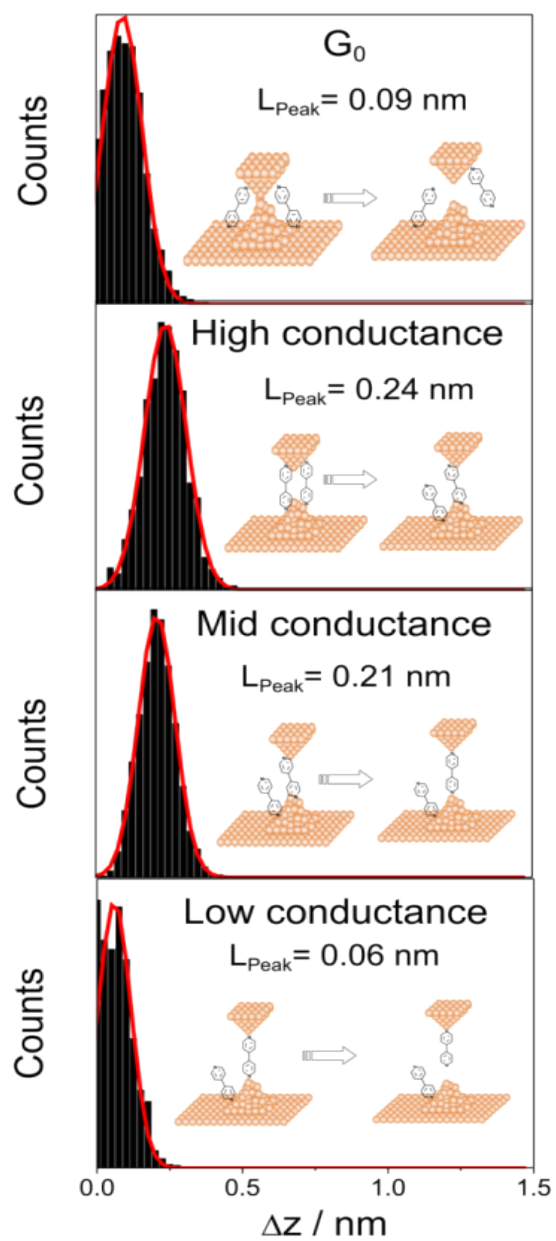


Figure S3. Plateau length histograms corresponding to each characteristic conductance (G_0 , H, M, and L). The peaks were fit to Gaussians to determine the most frequently observed plateau length in the individual traces.

2.3 Electrochemical gate effect at different pH values

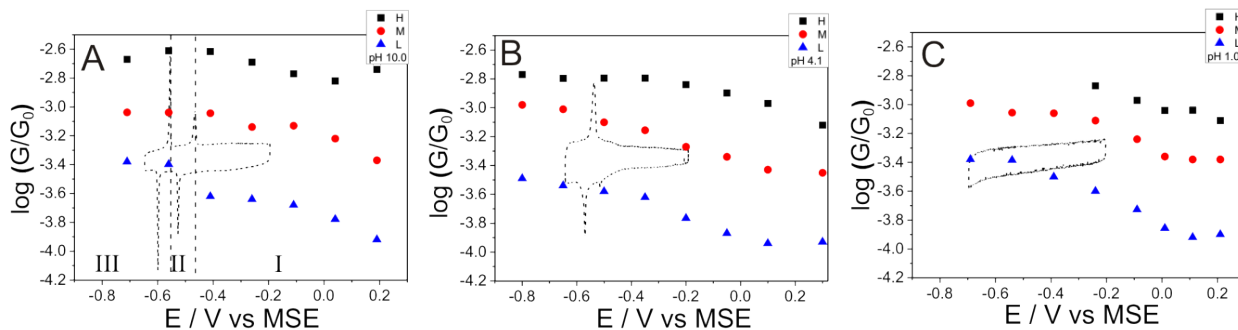


Figure S4. The most frequently measured conductance as a function of the applied electrode (STM substrate) potential for H, M, and L states at different pH values and cyclic voltammogram. The experiments were performed in (A) 0.05 M $\text{KClO}_4 + \text{NaOH}$ (B) 0.05 M $\text{KClO}_4 + \text{HClO}_4$ (C) 0.1 M HClO_4 containing 0.5mM 44BP. The bias voltage for all the measurements was kept at 100 mV.

2.4 π - π stacking evolution

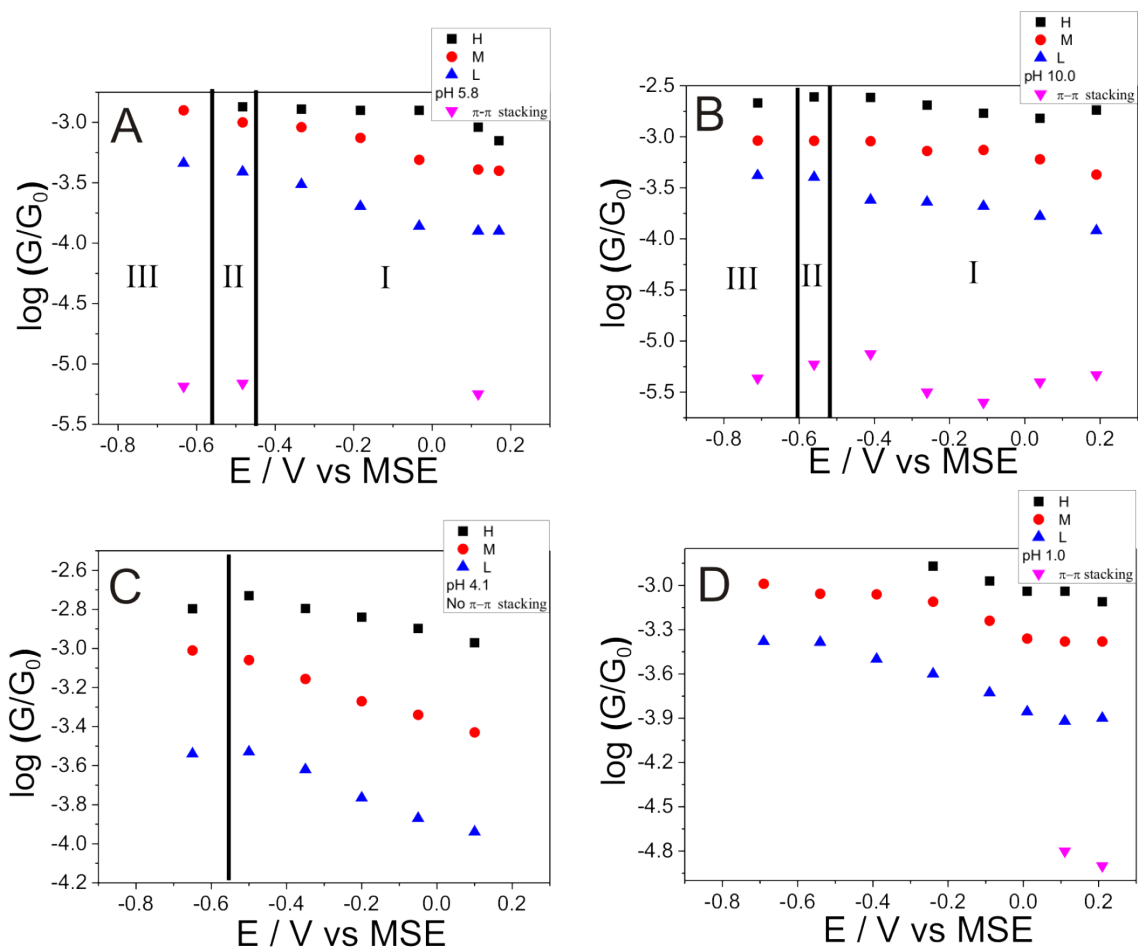


Figure S5. The most frequently measured conductance as a function of the applied electrode (STM substrate) potential for H, M, L, and π - π stacking states at different pH values. The experiments were performed in (A) 0.05 M

KClO₄. (B) 0.05 M KClO₄+ NaOH (C) 0.05 M KClO₄+ HClO₄ (D) 0.1 M HClO₄ containing 0.5mM 44BP. The bias potential for all the measurements was kept at 100 mV.

2.5 Comparison of gating efficiency with literature data

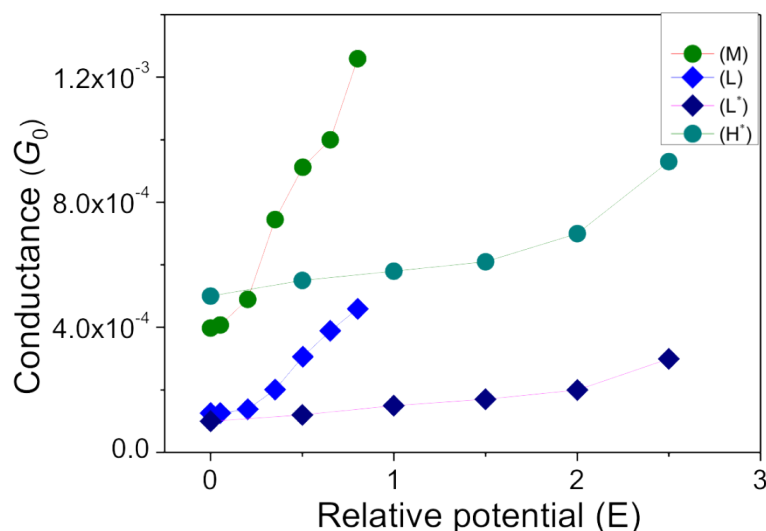


Figure S6. Comparison of electrochemical potential gating efficiency of 44BP. M, and L are medium and low conductance values using efficient gating control approach while H*, and L* are high and low conductance values of the same molecule published in the SI of ref [18], respectively.

3. DFT based electron transport calculations

Prior to junction model-geometry construction, a single isolated 44BP molecule was geometrically optimized with SIESTA, using DZP basis set, PBE exchange correlation functional parameterization, 300 Ry grid cutoff and 0.01eV/A force tolerance. The geometry optimization revealed that the optimal value of the N-N distance is 0.72nm for the isolated 44BP. The optimized 44BP geometry then was inserted between two opposing 111 directed 35-atom gold pyramids. The pyramids represent the tip of the electrodes shortly after the rupture of the last gold-gold bond between the two sides. To account for the three distinct configurations encountered during the elongation in the experiments, we chose three electrode separations: 0.76nm, 0.89nm and 1.09nm. The electrode separation is measured between the centers of the

apex atoms of the pyramids. For the shortest electrode separation, two molecules were placed between the pyramids, slightly asymmetrically, one molecule being closer to one of the pyramids than the other. In the two other cases with larger electrode separations only one molecule was placed between the pyramids. In the geometry construction, we were aiming to keep an approximate ~ 0.2 nm distance between the nitrogen and the closest gold atoms. Following this geometry construction, the structures were geometrically optimized with SIESTA using a DZP basis set, PBE exchange correlation functional parameterization, 300 Ry grid cut off and 0.01eV/A force tolerance. During the optimization, the bottom two layers of both pyramids, furthest away from the molecule were kept fixed and the periodic boundaries were set to 1nm larger in every dimensions than the size of the structure. As a result of this optimization, the electrode separations are changed slightly to 0.84nm, 0.96nm and 1.17nm. The typical N-Au bond length in the optimized junction geometries is around 0.22nm-0.23nm.

The transmission coefficient of the junction was calculated with a modified SMEAGOL[19] code (called GOLLUM) using the wide-band approximation, following the method described in ref[20]. The two wide-band leads were attached to the bottom base layers of the two pyramids with a Γ value of 4.0eV, using the notation and the value as in ref[20]. The Hamiltonian and overlap matrices were obtained with SIESTA using DZP basis set, PBE exchange correlation functional parameterization and 300 Ry grid cut off.

The electrochemical gating experiment gives a unique opportunity to readjust the bare-DFT provided resonance levels of the 44BP using a scissor correction[21]. For the scissor correction the molecular sub-block of the Hamiltonian matrix was modified: the molecular sub-Hamiltonian and overlap matrix were extracted and the corresponding eigenvalues were obtained. The eigenvalues below and above the bare-DFT computed Fermi energy (set as reference $E_F=0.0$ eV) were

shifted by ΔE_H and ΔE_L respectively. The shifted eigenvalues were then transformed back to its original basis, yielding the scissor corrected sub-Hamiltonian matrix, which was inserted back into the Hamiltonian matrix of the whole junction. The range of values for ΔE_H and ΔE_L were $\Delta E_H = -1 \dots 0 \text{eV}$ and $\Delta E_L = 0 \dots 1.9 \text{eV}$. It was found that the modification of the HOMO resonance did not change the transmission coefficient significantly in the vicinity of the Fermi energy and consequently we focused the LUMO resonance only. Figure S7 shows $T(E)$ with various ΔE_L values. Along with the DFT-based transmission coefficients, the figure also shows the fitted

Breit-Wigner curves,
$$T_{BW}(E, \Delta E_L) = \frac{4\Gamma_L \Gamma_R}{(E - \epsilon - \Delta E_L)^2 + (\Gamma_L + \Gamma_R)^2}$$
. The Γ_L , Γ_R and ϵ were fitted to the DFT-based $T(E)$ in the uncorrected, $\Delta E_L = 0 \text{eV}$ case (Figure S7 top-left panel). This fitting procedure was carried out for both L and M junction configuration, where the shape of $T(E)$ resembled a Lorentzian shape. For the M junction configuration the huge ratio between the couplings is due to asymmetric junction configurations that are likely occur in the experiment for electrode separations shorter than the molecular length. The smaller coupling can be attributed to gold-nitrogen coupling, and the larger coupling value corresponds to the gold- π system coupling.

The theoretically-estimated conductance values in the break-junction experiment were calculated as $G/G_0 = A T(E-E_g)$, where T denotes the corrected transmission coefficient. We find quantitative agreement between the DFT calculated and measured conductance values by choosing the LUMO correction in the range $\Delta E_L = 1.0 \dots 1.5 \text{eV}$ and the scaling factor $A=0.5$ (Figure 4 in the main text). The range of LUMO shifts agree with the recently publish results in ref [18, 22]. Figure S7 shows the transmission coefficients and the measured conductance values without the introduction of the scaling factor. It shows that by choosing larger than $\Delta E_L = 1.5 \text{eV}$

the quantitative agreement does not improve and demonstrate that better quantitative comparison can be found by an introduction of the scaling factor (see Figure 4.)

The top-right and bottom-left panels in Figure S7, where the LUMO correction are in the range $\Delta E_L = 1.0 \dots 1.5 \text{ eV}$, also demonstrate that both methods, i.e. the scissor-correction and the Lorentzian fitting suggest that a perfectly efficient gating increases the conductance about fourfold due to a Fermi energy shift in the experimental gate potential range. This trend matches well with the observed experimental modulation of the conductance. Furthermore Figure S6 shows a comparison with a recently published electrochemical gate experiment on 44BPy in ref [18] where the authors obtained a 1:5 electrochemical gate efficiency.

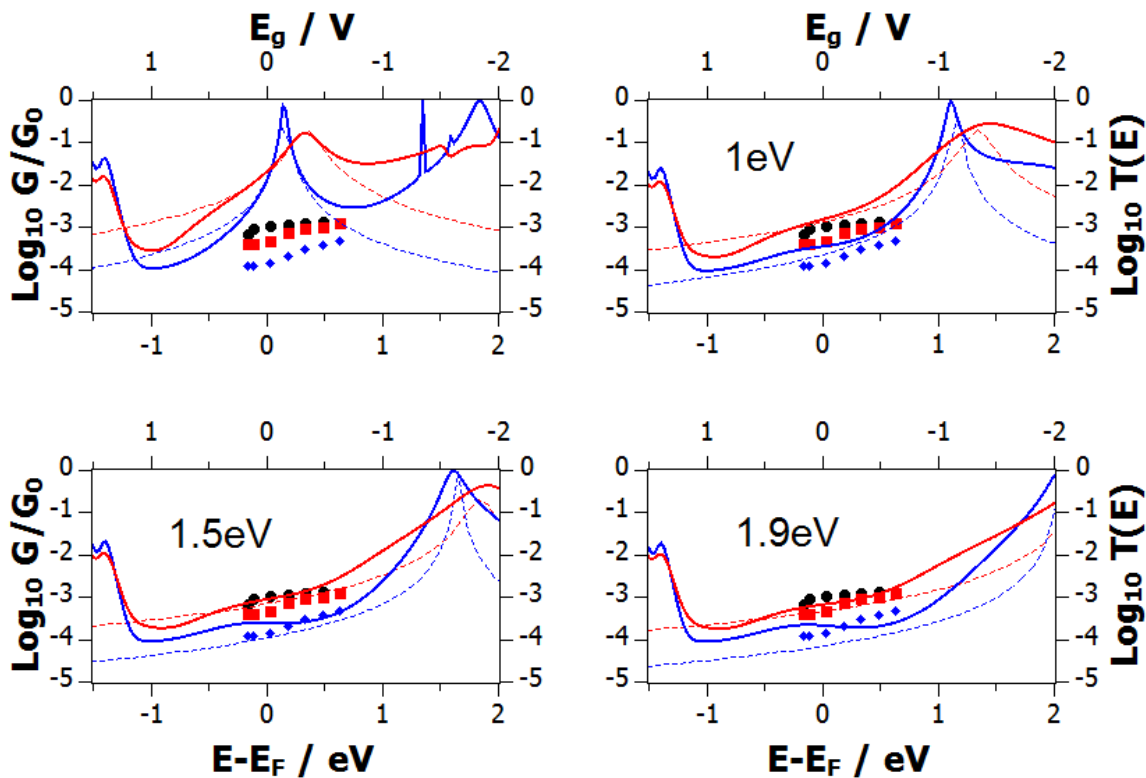


Figure S7. Transmission coefficient function and measured conductance against electrochemical gating potential for L (blue) and M (red) ranges. The transmission functions are with four different LUMO resonance: Top-left panel shows the uncorrected $T(E)$, Top-right panel shows $T(E)$ where the LUMO energy of the molecule were shifted by 1 eV. The bottom panels show also the corrected $T(E)$ with 1.5 eV and 1.9 eV LUMO shifts, respectively. The dashed

curves show the fitted and shifted Bright--Wigner curves. For junction L, $\Gamma_L=\Gamma_R=0.008\text{eV}$ and $\epsilon=0.15\text{eV}$. For junction M, $\Gamma_L=0.006\text{eV}$, $\Gamma_R=0.109\text{eV}$ and $\epsilon=0.34\text{eV}$.

4. Reference

1. Li, C., et al., *Charge Transport in Single Au | Alkanedithiol | Au Junctions: Coordination Geometries and Conformational Degrees of Freedom*. Journal of the American Chemical Society, 2007. **130**(1): p. 318-326.
2. Gábor, M., et al., *Current measurements in a wide dynamic range—applications in electrochemical nanotechnology*. Nanotechnology, 2007. **18**(42): p. 424004.
3. Yanson, A.I., et al., *Formation and manipulation of a metallic wire of single gold atoms*. Nature, 1998. **395**(6704): p. 783-785.
4. Trouwborst, M.L., et al., *Single atom adhesion in optimized gold nanojunctions*. Physical Review Letters, 2008. **100**(17).
5. Huisman, E.H., et al., *Stabilizing Single Atom Contacts by Molecular Bridge Formation*. Nano Letters, 2008. **8**(10): p. 3381-3385.
6. Quek, S.Y., et al., *Mechanically controlled binary conductance switching of a single-molecule junction*. Nature Nanotechnology, 2009. **4**(4): p. 230-234.
7. Mishchenko, A., et al., *Single-Molecule Junctions Based on Nitrile-Terminated Biphenyls: A Promising New Anchoring Group*. Journal of the American Chemical Society, 2011. **133**(2): p. 184-187.
8. Martin, C.A., et al., *Fullerene-based anchoring groups for molecular electronics*. Journal of the American Chemical Society, 2008. **130**(40): p. 13198-13199.
9. Hong, W., et al., *Single Molecular Conductance of Tolanes: Experimental and Theoretical Study on the Junction Evolution Dependent on the Anchoring Group*. Journal of the American Chemical Society, 2012. **134**(4): p. 2292-2304.
10. Wang, C., et al., *Oligoynes Single Molecule Wires*. Journal of the American Chemical Society, 2009. **131**(43): p. 15647-15654.
11. Kamenetska, M., et al., *Conductance and Geometry of Pyridine-Linked Single-Molecule Junctions*. Journal of the American Chemical Society, 2010. **132**(19): p. 6817-6821.
12. Rubio, G., N. Agrait, and S. Vieira, *Atomic-sized metallic contacts: Mechanical properties and electronic transport*. Physical Review Letters, 1996. **76**(13): p. 2302-2305.
13. Torres, J.A. and J.J. Saenz, *Conductance and mechanical properties of atomic-size metallic contacts: A simple model*. Physical Review Letters, 1996. **77**(11): p. 2245-2248.
14. Sanchez-Portal, D., et al., *Stiff monatomic gold wires with a spinning zigzag geometry*. Physical Review Letters, 1999. **83**(19): p. 3884-3887.
15. Xu, B.Q., X.Y. Xiao, and N.J. Tao, *Measurements of single-molecule electromechanical properties*. Journal of the American Chemical Society, 2003. **125**(52): p. 16164-16165.
16. Velez, P., S.A. Dassie, and E.P.M. Leiva, *First principles calculations of mechanical properties of 4,4'(-)bipyridine attached to Au nanowires*. Physical Review Letters, 2005. **95**(4).
17. Huang, Z., et al., *Single molecule junctions formed via au-thiol contact: Stability and breakdown mechanism*. Journal of the American Chemical Society, 2007. **129**(43): p. 13225-13231.
18. Capozzi, B., et al., *Tunable Charge Transport in Single-Molecule Junctions via Electrolytic Gating*. Nano Letters, 2014. **14**(3): p. 1400-1404.
19. Rocha, A.R., et al., *Spin and molecular electronics in atomically generated orbital landscapes*. Physical Review B, 2006. **73**(8): p. 085414.

20. Verzijl, C.J.O., J.S. Seldenthuis, and J.M. Thijssen, *Applicability of the wide-band limit in DFT-based molecular transport calculations*. The Journal of chemical physics, 2013. **138**(9): p. 094102.
21. García-Suárez, V.M. and C.J. Lambert, *First-principles scheme for spectral adjustment in nanoscale transport*. New Journal of Physics, 2011. **13**(5): p. 053026.
22. Kim, T., et al., *Determination of Energy Level Alignment and Coupling Strength in 4,4' - Bipyridine Single-Molecule Junctions*. Nano Letters, 2014. **14**(2): p. 794-798.